

A study of the impact of the Intertropical Convergence Zone on aerosols during INDOEX

C. Andronache

Atmospheric and Environmental Research Inc., Lexington, Massachusetts, USA

L. J. Donner, C. J. Seman, and R. S. Hemler

Geophysical Fluid Dynamics Laboratory, NOAA, Princeton University, Princeton, New Jersey, USA

Received 29 September 2000; revised 11 January 2001; accepted 13 June 2001; published 11 September 2002.

[1] We report model simulations of the effect of deep convection on aerosol under typical Intertropical Convergence Zone (ITCZ) conditions in the tropical Indian Ocean as encountered during the Indian Ocean Experiment (INDOEX). Measurements taken during various phases of INDOEX showed significant aerosol mass concentrations of nss-sulfate, carbonaceous, and mineral dust over the northern Indian Ocean. During the winter dry season these aerosol species accumulate and are transported long distances to the tropical regions. In contrast, aerosol measurements south of the ITCZ exhibit significantly lower aerosol concentrations, and the convective activity, mixing, and wet removal in the ITCZ are responsible for their depletion. Our results, based on a cloud-resolving model, driven by National Centers for Environmental Prediction analysis, show that convection and precipitation can remove significant amounts of aerosol, as observed in the Indian Ocean ITCZ. The aerosol lifetime in the boundary layer (BL) is of the order of hours in intense convection with precipitation, but on average is in the range of 1–3 days for the case studied here. Since the convective events occur in a small fraction of the ITCZ area, the aerosol lifetime can vary significantly due to variability of precipitation. Our results show that the decay in concentration of various species of aerosols is comparable with in situ measurements and that the ITCZ can act to reduce the transport of polluted air masses into the Southern Hemisphere especially in cases with significant precipitation. Another finding is that aerosol loading typical to north of ITCZ tends to induce changes in cloud microphysical properties. We found that a difference between clean air masses as those encountered south of the ITCZ to aerosol polluted air masses as encountered north of the ITCZ is associated with a slight decrease of the cloud droplet effective radius (average changes of about $2 \mu\text{m}$) and an increase in cloud droplet number concentration (average changes by about 40 to 100 cm^{-3}) consistent with several in situ measurements. Thus polluted air masses from the northern Indian Ocean are associated with altered microphysics, and the extent of these effects is dependent on the efficiency of aerosol removal by ITCZ precipitation and dilution by mixing with pristine air masses from the Southern Hemisphere.

INDEX TERMS: 0305 Atmospheric Composition and Structure: Aerosols and particles (0345, 4801); 0345 Atmospheric Composition and Structure: Pollution—urban and regional (0305); 0368 Atmospheric Composition and Structure: Troposphere—constituent transport and chemistry; 0365 Atmospheric Composition and Structure: Troposphere—composition and chemistry **KEYWORDS:** INDOEX, tropospheric aerosols, ITCZ, indirect effect, aerosol removal, aerosols and clouds

Citation: Andronache, C., L. J. Donner, C. J. Seman, and R. S. Hemler, A study of the impact of the International Convergence Zone on aerosols during INDOEX, *J. Geophys. Res.*, 107(D19), 8027, doi:10.1029/2001JD900248, 2002.

1. Introduction

[2] Observations taken during various phases of the Indian Ocean Experiment (INDOEX) show that polluted air masses from the sub-Indian continent can travel to the Intertropical Convergence Zone (ITCZ) within 6–7 days [Collins *et al.*, 2002]. Under the winter monsoon circulation the continental aerosols, typically non-sea-salt sulfate (nss-sulfate), carbonaceous particles, and mineral dust, are transported by the northeasterly winds toward the Arabian Sea and the tropical Indian

Ocean [Prospero, 1979; Krishnamurti *et al.*, 1998; Jayaraman *et al.*, 1998; Ramanathan *et al.*, 1996; Bates *et al.*, 2002; Ansmann *et al.*, 2000; P. Rasch *et al.*, unpublished manuscript, 2000]. Increased aerosol concentration over large areas of the Indian Ocean provides a significant perturbation to the marine “background” aerosol loading, and it has been demonstrated that part of the continental aerosol is of anthropogenic origin [Satheesh *et al.*, 1999; Podgorny *et al.*, 2000; Guazzotti *et al.*, 2001; Muller *et al.*, 2000; M. Norman *et al.*, unpublished manuscript, 2000]. One of the primary goals of the overall INDOEX experiment is to assess the direct and indirect radiative effects of aerosols and their interactions with clouds. It has been

Table 1. Aerosol Mass Concentration Over Equatorial Indian Ocean During 1987–1999

Location	Nss-Sulfate	Sodium	Mineral Dust	Carbonaceous	Source ^a
South of ITCZ	0.1–0.5	1.9	<0.1	N	1
	0.5 (0.17)	2.9 (1.0)	0.27 (0.2)	N	2
	0.6	1.0–2.0	<0.1	<0.1	3
	0.1–0.3	N	N	0.6	4
	0.1	2.0	0.01	0.6	5
North of ITCZ	1.0–4.0	1.9	~1.0	N	1
	1.14 (0.75)	2.4 (1.2)	1.01 (0.81)	N	2
	1.0–3.0	1.0–2.0	0.1–1.0	0.3–0.6	3
	0.3–1.6	N	N	1.5	4
	4.0	2.0	1.0	1.5	5

^aSources: 1, *Krishnamurti et al.* [1998]; 2, *Savoie et al.* [1987]; 3, *Clarke et al.* [2002]; 4, *Cantrell et al.* [2000]; 5, typical values used for model initializations. Values represent mean and standard deviations in $\mu\text{g m}^{-3}$. All data correspond to the low-dust conditions. N indicates lack of data.

reported that significant radiation absorption caused by carbon particles originating from biomass burning and combustion can cause a reduction of low-level clouds over Indian Ocean with possible impact on large-scale circulation [*Ackerman et al.*, 2000]. Other studies argue that the efficient transport of aerosols during winter monsoon might provide a significant aerosol source for the Southern Hemisphere (SH) atmosphere [*Moody et al.*, 1991; *Krishnamurti et al.*, 1998].

[3] Earlier studies indicated that deep convective systems transport chemical species from the atmospheric boundary layer (BL) into the free and upper troposphere [*Chatfield and Crutzen*, 1984; *Wang and Crutzen*, 1995; *Taylor et al.*, 1997; *Mari et al.*, 2000]. While the long-range transport of aerosol in the northern Indian Ocean tends to preserve large aerosol loading in the BL, once these air masses reach the ITCZ region, particles are lifted into free tropospheric regions by deep convective motions and are efficiently removed by precipitation. Since ITCZ has significant cloud cover [*Warren et al.*, 1988] and significant probability of precipitation, aerosols can influence the cloud microphysical and optical properties. The duration and the intensity of these effects in the ITCZ clouds are in part dependent on how efficient particles are removed from the atmosphere. The representation of scavenging and deposition processes in current models remains an important task [*Rasch et al.*, 2000], and INDOEX data provided the opportunity to simulate in detail the evolution of aerosol mass concentration of various species under convective activity.

[4] We use a high-resolution cloud-resolving model constrained by INDOEX and National Centers for Environmental Prediction (NCEP) data to simulate the evolution of several aerosol species under precipitation and mixing specific to Indian Ocean ITCZ. The goals of this study are to provide insight into aerosol decay in the ITCZ as well as to estimate possible alteration of cloud microphysical properties by polluted air masses. We employ a detailed representation of aerosol removal by precipitation and compare model results with available observations taken during INDOEX. First, we present an overview of the aerosol and meteorological data for the case studied here. Then we describe the method used to simulate the depletion of aerosols by precipitation and dilution in our cloud-resolving model. Finally, we show simulations of aerosol concentration evolution during three days in the Indian Ocean ITCZ under convective activity and precipitation, and we discuss the impact of aerosols on cloud microphysics.

2. Observational Data

2.1. Aerosol Data

[5] For the purposes of this modeling study, we compiled data taken north of the ITCZ and south of the ITCZ during INDOEX ship measurements [*Savoie et al.*, 1987; *Krishnamurti et al.*, 1998; *Clarke et al.*, 2002; *Cantrell et al.*, 2000]. All aerosol data refer to winter monsoonal circulation conditions that exhibit enhanced aerosol concentrations extended southward into the tropical Indian Ocean. There were reported several aerosol species that are now considered typical for this environment: sea salt that has a local source at the ocean surface and that is function of meteorological conditions; non-sea-salt sulfate (nss-sulfate) which has primary sources on the continent, with additional secondary source from gas and aqueous phase oxidation of sulfur dioxide (SO_2); mineral dust with contributions from the sub-Indian continent, Arabian Peninsula, and Africa; and carbonaceous aerosol with sources from biomass burning and anthropogenic activities. The data used are based on reported measurements during 14 January to 23 March 1979 on board of R/V *Salerum*, R/V *Iselin*, and R/V *Researcher* [*Savoie et al.*, 1987], during 5 January to 4 February 1996 on board of R/V *Sagar Kanya* [*Krishnamurti et al.*, 1998], February–March 1998 on board of R/V *Sagar Kanya* [*Cantrell et al.*, 2000], and February–March 1999 on board of R/V *Ron Brown* [*Clarke et al.*, 2002; *Dickerson et al.*, 2002]. A concise overview of these data is given in Table 1. A predominant feature of these data is a large contrast in the concentrations of nss-sulfate, carbonaceous, and mineral dust aerosols between north and south of the ITCZ. The sea-salt component which defines the background MBL aerosol in pristine SH Indian Ocean is assumed to be at the same levels across the ITCZ, although significant variability was observed. Our focus is to understand the role of excess nss-sulfate, carbon, and mineral dust in the ITCZ clouds, and the removal of these aerosols as the air masses interact with the ITCZ.

[6] The model simulations described in this paper require information on the aerosol loading (such as aerosol mass concentration) and size distribution parameters. The aerosol mass concentrations for initial and boundary conditions are taken from observations (Table 1), and the other size distribution parameters (geometric mean diameter, geometric standard deviation, and density) for the species of interest here are taken from *d’Almeida et al.* [1991] and are shown in Table 2. We made some simplifying assumptions regarding the structure of aerosol: sea salt is predominant in accumulation and coarse

Table 2. Aerosol Species and Size Distribution Parameters Used in Model Simulations

Aerosol Species	d_{pg} , μm	σ_g	Density, kg m^{-3}	Comments ^a
Nss-sulfate (acm)	0.137	2.03	1700	1
Sea salt (acm)	0.417	2.03	2200	2
(com)	3.512	2.03	2200	
Carbonaceous (num)	0.023	2.00	1000	3
Mineral dust (acm)	0.757	2.00	2600	4

^aComments: 1, acm accumulation mode; num, nucleation mode; com, coarse mode; nss-sulfate is assumed predominant in acm mode; 2, sea salt in accumulation and coarse modes are dominant; 3, fine carbonaceous particles can be transported long distances; 4, accumulation mode of mineral dust is dominant. Here d_{pg} is the geometric mean diameter; σ_g is the geometric standard distribution; parameters are taken from *d'Almeida et al.* [1991].

mode, nss-sulfate is represented as an accumulation mode (while nucleation mode can exist, it is much smaller than the continental source), carbon particles are generally fine and are

represented in a nucleation mode, and the mineral dust is approximated by an accumulation mode (the coarse mode caused by intense transport from desert is more typical near coastal regions).

2.2. Meteorological Data

[7] Meteorological conditions north of the ITCZ region during INDOEX are generally characterized by southward flow, low or absent precipitation, and somewhat intense convective precipitation in the ITCZ domain. A summary picture of these conditions is provided by the time-average vertical soundings taken on board of *Ron Brown* ship during 16–18 March 1999, in the latitude interval 3°N to 10°S (Figure 1). The ship traveled across the ITCZ with small variations in longitude (~72°E to 75°E). The soundings were taken with a frequency of about four per day, but only the average and one standard deviation are shown here. We observe a consistent zonal westerly flow in the lower and midtroposphere up to about 6 km, and easterly in the upper troposphere (Figure 1a). The meridional flow indicates predominant southward trans-

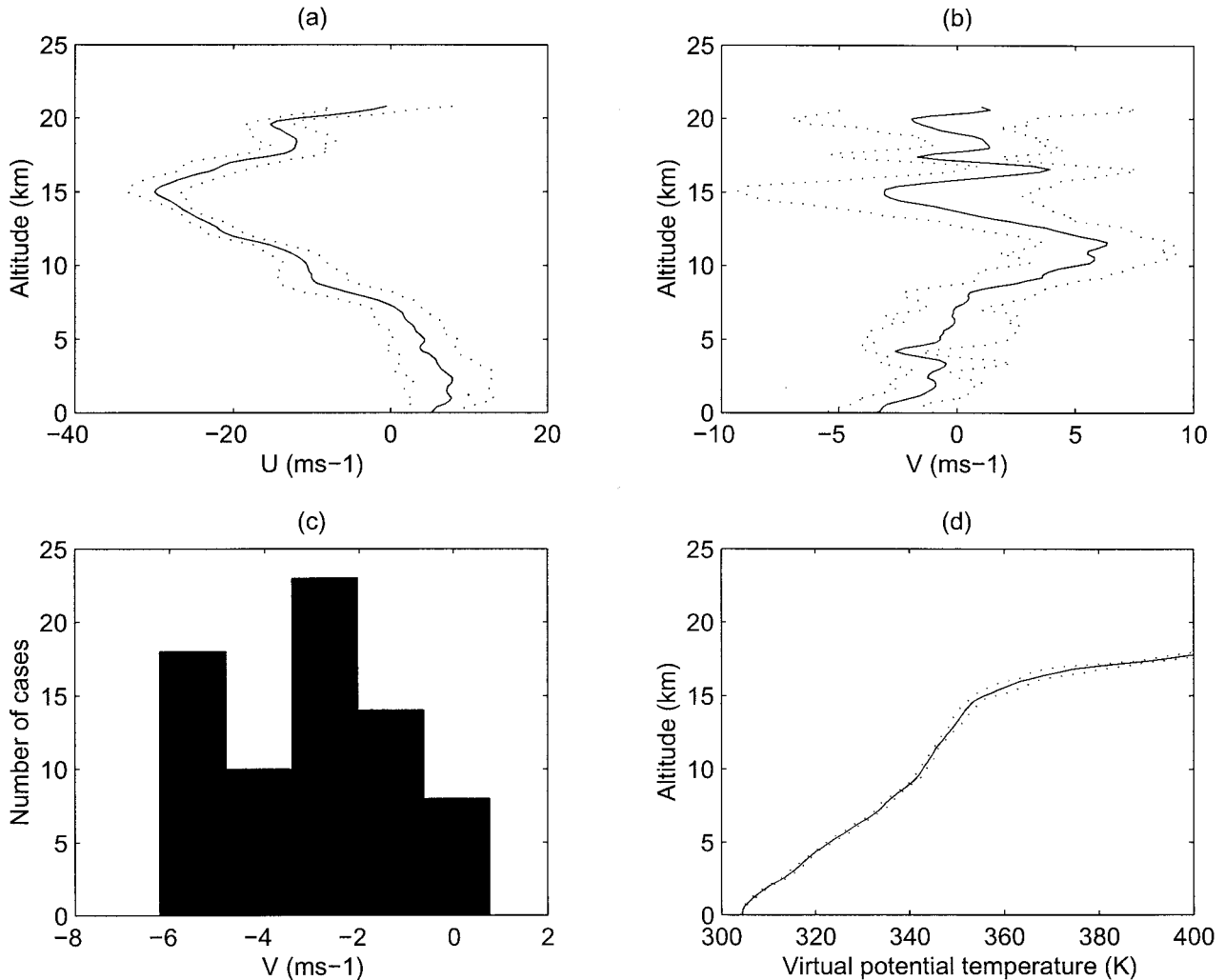


Figure 1. Vertical average profiles of (a) zonal wind U , (b) meridional wind V , (c) histogram of the meridional wind component V for $z < 1$ km, and (d) virtual potential temperature θ_v , for the time interval 16–18 March 1999, based on soundings taken from *Ron Brown* ship between latitudes 5°N–10°S and longitudes 72°E–75°E. The averages are shown by solid lines, and one standard deviation departures are shown by dotted lines.

port in the lower troposphere (Figure 1b). During this time interval the ship traveled southward about 13° of latitude and had an average speed of $\sim 5 \text{ m s}^{-1}$. On average, this speed is slightly higher than the southward airspeed, given by the meridional velocity V in the first kilometer near the ocean surface, as shown by the histogram in Figure 1c. The average of V in the first kilometer is -2.8 m s^{-1} with a standard deviation of 1.8 m s^{-1} . Figure 1d shows the average profile virtual potential temperature and departures by one standard deviation.

[8] The meteorological data required by the LAN model consist of initial conditions given by vertical soundings and large-scale forcing of moisture, potential temperature, and wind, which can be calculated using vertical soundings at the domain boundaries. We use the NCEP-analyzed meteorological data to provide these conditions for a case study of 16–18 March 1999 at 5°S – 72°E . The case was selected to correspond with significant convective activity in the Indian Ocean ITCZ, and with the passage of *Ron Brown* vessel from north to south of the ITCZ. During this passage, aerosol measurements showed a large concentration gradient across the ITCZ, and the backward air mass trajectories indicated long-range transport of airflow from the northern Indian Ocean into the ITCZ area where particles are presumably mixed in cleaner air masses or removed by precipitation [Cantrell *et al.*, 2000; Dickerson *et al.*, 2002].

3. Modeling Approach

[9] We explore the removal of aerosols in the ITCZ Indian Ocean using the limited area non-hydrostatic (LAN) model developed at the Geophysical Fluid Dynamics Laboratory (GFDL). LAN is a high-resolution dynamic cloud-resolving model designed for studies of aerosols, clouds, radiative-convective equilibrium, and aerosol-clouds interactions [Lipps and Hemler, 1986; Held *et al.*, 1993; Donner *et al.*, 1999; Andronache *et al.*, 1999]. The model provides a framework for studies of aerosols and clouds and employs physics typical for a high-resolution mesoscale model with elastic dynamics, bulk microphysics, and interactive radiation (for details, see Held *et al.* [1993]). The model cloud physics scheme predicts the water concentration in gas phase, cloud droplets, snow, and rain. The radiation code is a 56-band two-stream δ -Eddington scheme, modified to include gaseous absorption and a parameterization for Rayleigh scattering and cloud optical properties [Ramaswamy and Kiehl, 1985; Slingo, 1989]. A two-dimensional version of the model is used in this study, and the model resolutions are horizontal resolutions of 2 km, vertical resolution of 500 m, and temporal resolution of 1 s. The model domain covers 128 km horizontally, 21 km vertically, and the duration of simulated time is 3 days.

3.1. Cloud Microphysics Scheme

[10] The model employs a bulk cloud physics with prognostic equations for four variables of interest: q_v , water vapor mixing ratio; q_c , cloud water/ice mixing ratio; q_s , snow mixing ratio; and q_r , rainwater mixing ratio. The governing equations for each variable, and the assumptions made in the parameterization of the main microphysical processes are described by Held *et al.* [1993]. The cloud-water mixing ratio q_c represents both the water and cloud ice, and its partition into liquid and ice phase is parameterized as a function of temperature. For temperatures greater than -6°C , q_c is assumed to be cloud water only, and the heat of vaporization is released at conden-

sation. For temperatures less than -12°C , q_c is assumed to be ice only, and the latent heat of sublimation is released at condensation. At intermediate temperatures a mixture of cloud water and ice is considered, with the percentage of each component varying linearly with temperature [Lord *et al.*, 1984]. Although this approach was consistently used in previous studies with LAN, we must note that generally supercooled liquid water droplets can exist at lower temperatures than -12°C and that ice formation has a complex dependence on cloud microphysical processes that are not explicitly represented in bulk cloud schemes [Hobbs and Rangno, 1985].

[11] The parameterization of the cloud optical properties requires the cloud droplet effective radius r_e and the cloud water path (CWP). For each spectral interval i the optical thickness τ_i , the single scattering albedo ω_p , and the asymmetry parameter g_i can be linked to CWP and r_e [Slingo, 1989; Ebert and Curry, 1992]. It must be noted that recent direct measurements of g_i in visible tend to give lower values than the models and this can have implications for long-term integration of cloud models [Garrett *et al.*, 2001]. The cloud droplet effective radius r_e is estimated from q_c and the cloud droplet number concentration N_d , which is linked to aerosol concentration at cloud base and the local updraft velocity W [Ghan *et al.*, 1997]. The model was used in previous studies to simulate convective activity, water cycle, and aerosol effects on clouds for the Global Atmosphere Tropical Experiment (GATE) and Tropical Ocean Global Atmosphere Coupled Ocean Atmosphere Response Experiment (TOGA COARE) data [Lipps and Hemler, 1986; Held *et al.*, 1993; Haywood *et al.*, 1997; Donner *et al.*, 1999].

3.2. Aerosol Scheme

[12] The aerosol-cloud interaction model used in this work follows closely the concepts developed by Hegg *et al.* [1984] for sulfate aerosol, and the scheme was extended to include the main aerosol species that are important for the ITCZ Indian Ocean. A complex range of processes contribute to changes of the “dry” aerosol mixing ratio of a given aerosol species, denoted x_i , where $i=1, 4$ (1, nss-sulfate; 2, carbonaceous; 3, mineral dust; and 4, sea salt). By dry aerosol we denote the aerosol particles at RH $\sim 40\%$, and the size of aerosol particles varies with the ambient relative humidity (RH) [Quinn *et al.*, 1993; Baumgardner and Clarke, 1998; Fitzgerald *et al.*, 1998]. Changes in x_i are induced by transport, sources, and sinks. The continuity equation for x_i is

$$\frac{\partial(\rho_0 x_i)}{\partial t} = ADV + DIFF + P_i - D_i, \quad (1)$$

where ρ_0 is the air density, ADV are the advection terms, $DIFF$ are the diffusion terms, P_i are the production terms, and D_i are the destruction (or loss) terms of x_i . Several important simplifications are possible for our study of aerosol removal due to the specific location of the domain of integration in the ITCZ, where the dominant term is removal of aerosols by precipitation. The production term is assumed negligible for carbonaceous and mineral dust aerosols because the main sources of these aerosols are continental. The sea-salt production is parameterized as a function of the horizontal wind intensity near the surface, U , following the treatment by O’Dowd *et al.* [1999].

[13] The nss-sulfate has three possible sources described by three rates of production: P_1 , the rate of sulfate formation by SO_2 oxidation in gas phase with deposition of H_2SO_4 on pre-

existent particles; P_2 , rate of sulfate formation by SO_2 aqueous oxidation followed by droplet evaporation; P_3 , rate of sulfate formation by nucleation of new particles from H_2SO_4 , water and possible other gaseous species [Weber *et al.*, 1997]. Extensive previous research indicates that P_1 is about $0.8\% \text{ h}^{-1}$, and P_2 is about $2\text{--}4\% \text{ h}^{-1}$ [Scott, 1982; Warneck, 1988; Flossmann *et al.*, 1987]. The rate of in-cloud conversion of SO_2 into sulfate is considerably larger than the gas phase conversion of SO_2 into particulate phase, a fact supported by many observations [Hegg *et al.*, 1984]. Nevertheless, given the fact that cloud cover in the ITCZ is intermittent and the deep convective clouds cover only $5\text{--}10\%$ of the domain, P_1 and P_2 are comparable in importance, but they are much smaller than the wet removal rate, since about $95\% \text{ h}^{-1}$ can be removed by rain [Flossmann *et al.*, 1987]. Generally, P_3 is much smaller than P_1 and has a sporadic character since nucleation is possible only at high H_2SO_4 concentrations, high RH and low ambient preexistent aerosol background or in cloud outflow [Weber *et al.*, 1997]. While these rates can have significant variability, for an area with intense convection and precipitation, they tend to be much smaller than the removal rate of aerosol transported in the region.

[14] The loss D_i is caused by dry deposition and by wet deposition. The dry deposition of aerosols is predominant over clear sky of the northern Indian Ocean during the winter monsoon, and is treated following Slinn *et al.* [1978]. The wet deposition contains two major terms: one due to below-cloud aerosol particle collection by falling raindrops, and the second is due to the transfer of aerosol from cloud droplets into raindrops, when the rain is formed. The below-cloud aerosol particle collection by raindrops is described in detail in the next subsection. The transfer of aerosol from cloud water into rainwater is given by $f\epsilon x_i$, where $f = (S_{ar} + S_{cr})/q_c$ is the fraction of cloud water converted in rainwater and ϵ is the efficiency of aerosol scavenging by cloud droplets. S_{ar} is the rate of auto-conversion of cloud water into rainwater, and S_{cr} is the rate of accretion or collection, describing the collection of cloud droplets by raindrops [see Held *et al.*, 1993]. The in-cloud scavenging combines the effects of nucleation scavenging, attachment of particles to cloud droplets by Brownian motion, and collisional capture [Pruppacher and Klett, 1998]. From these three processes the nucleation scavenging has the most important effect upon mass concentration. The Brownian scavenging and the collisional capture of interstitial particles by cloud droplets are less efficient scavenging processes. Their efficiency is higher for small particles, which has little consequence for the mass concentration but can change the number size distribution [Flossmann and Pruppacher, 1988]. On the basis of extensive measurements it has been determined that for marine clouds $\epsilon \sim 0.95$ [Warneck, 1988] a value that is considered in our study for all aerosol species. Here we assume that all aerosols transported from continent into the ITCZ area are wettable and have hygroscopic properties. The dust and carbonaceous particles are aged during their long-range transport of several days, and they are likely to be coated or mixed with hygroscopic substances [Seinfeld and Pandis, 1998]. However, the possibility of a less efficient scavenging of carbonaceous particles into cloud droplets must be considered in regions close to the source.

3.2.1. Aerosol Removal by Rain

[15] While most of the aerosol mass is incorporated in cloud droplets, these particles are not removed from the atmosphere until precipitation takes place. For the ITCZ region

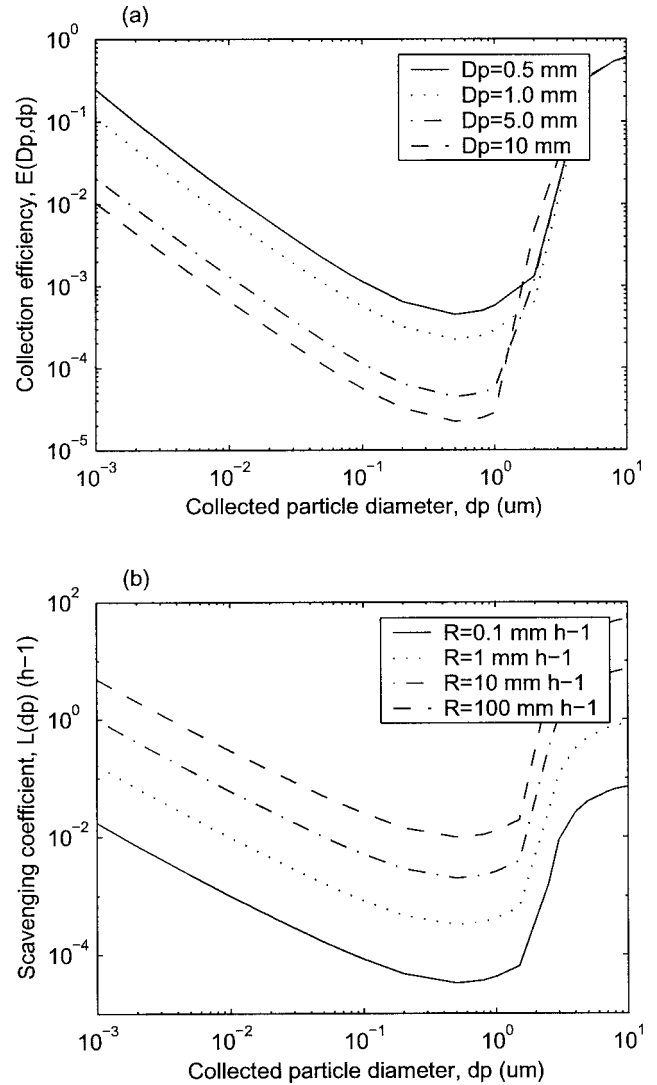


Figure 2. (a) Collection efficiency of aerosol particles of diameter d_p by raindrop of diameter D_p and (b) scavenging coefficient of aerosol particles due to a Marshall-Palmer raindrop size distribution for several precipitation rates R .

the precipitation scavenging is the most efficient process of particulate removal, a fact demonstrated by recent INDOEX field measurements that show a dramatic gradient in aerosol concentrations across the ITCZ [Savoie *et al.*, 1987; Rhoads *et al.*, 1997; Cantrell *et al.*, 2000; Dickerson *et al.*, 2002]. Given the importance of this process and the fact that aerosol and raindrop size distributions are known fairly well, we can represent in detail the rate of aerosol removal. A mean mass scavenging coefficient due to aerosol removal by raindrop collection, L_m , can be defined by

$$\frac{\partial(\rho_0 x)}{\partial t} = -L_m(\rho_0 x), \quad (2)$$

where x is the aerosol mixing ratio. L_m can be expressed as

$$L_m = \frac{\int_0^\infty L(d_p) d_p^2 n(d_p) dd_p}{\int_0^\infty n(d_p) d_p^3 dd_p}, \quad (3)$$

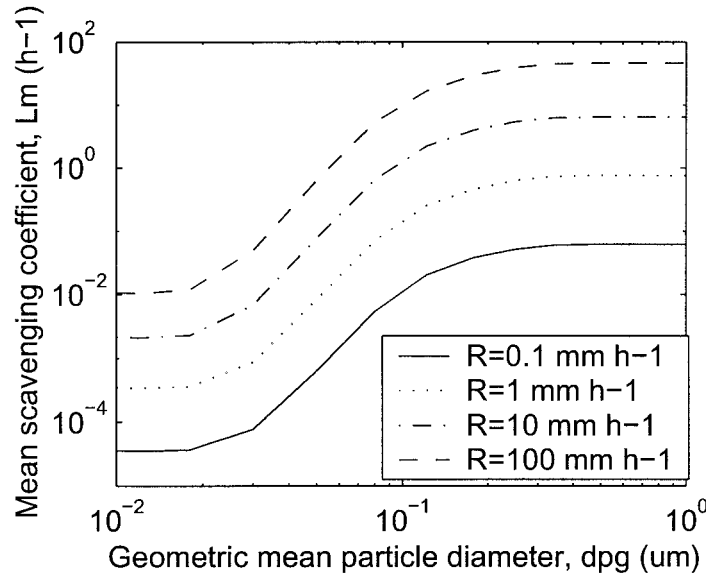


Figure 3. Mean mass scavenging coefficient of aerosol versus the geometric mean particle diameter d_{pg} for four precipitation rates.

where $n(d_p)$ is the aerosol size distribution and $L(d_p)$ is the scavenging coefficient of a particle of diameter d_p by rain. This scavenging coefficient is given by

$$L(d_p) = \int_0^\infty (\pi/4) D_p^2 U_i(D_p) E(D_p, d_p) N_D(D_p) dD_p, \quad (4)$$

where $E(D_p, d_p)$ is the collection efficiency between a raindrop of diameter D_p and an aerosol particle of diameter d_p , $U_i(D_p)$ is the terminal velocity of a raindrop, and $N_D(D_p)$ is the raindrop size distribution [Slinn, 1984].

[16] For a given raindrop diameter the collision efficiency E is dominated by Brownian diffusion for small aerosol particles ($d_p < 0.1 \mu\text{m}$), and by inertial impaction for large particles ($d_p > 1 \mu\text{m}$). Thus, for a given size of raindrop diameter, the scavenging of small and large aerosol particles is more efficient, while particles in the 0.1 to 1.0 μm size range are scavenged relatively slow (Figure 2a). We also note that smaller raindrops are more efficient in scavenging aerosol particles of a given diameter as long as the aerosol particle diameter is less than $\sim 1 \mu\text{m}$. Raindrops have a size distribution approximated by the Marshall-Palmer (MP) size distribution, $N_D = N_0 \exp(-bD_p)$, where $N_0 = 0.08 \times 10^{-8} \text{ m}^{-4}$ and $b = 1/\langle D_p \rangle$, with $\langle D_p \rangle$ the average raindrop diameter [Marshall and Palmer, 1948]. In turn, $\langle D_p \rangle = 0.01 \times R^{0.21/41}$, where R is the rate of rainfall in units of mm h^{-1} . The aerosol is represented by a lognormal size distribution,

$$n(d_p) = \frac{N}{(2\pi)^{1/2} d_p \log(\sigma_g)} \exp\left(-\frac{\log^2(d_p/d_{pg})}{2\log^2(\sigma_g)}\right), \quad (5)$$

where N is the total aerosol concentration, d_{pg} is the geometric mean diameter, and σ_g is the geometric standard deviation. The effect of scavenging of aerosol particles by a rain described by MP size distribution, is shown in Figure 2b. We note similarities with E and an increase of the scavenging with the precipitation rate R , which translates in shorter aerosol lifetime for higher precipitation rates. (The rainwater mixing ratio q_r is related to the rain intensity R by the relation $R =$

$4k\langle D_p \rangle q_r \rho_0 / \rho_w$, where k is a factor in the relation $U_i(D_p) = kD_p$, ρ_w is the water density, ρ_0 is the air density, and $\langle D_p \rangle$ is the mean diameter of raindrops for a MP raindrop size distribution.)

[17] In order to apply one scavenging coefficient for the mass concentration of aerosol of a given species, we use the mean mass scavenging coefficient L_m as defined above. Thus L_m depends on the rain size distribution (through R , the precipitation rate), and on the aerosol size distribution parameters (the geometric mean diameter d_{pg} and the geometric standard deviation σ_g). From the aerosol data for INDOEX we found that the variations of σ_g were relatively small but there is significant variability of d_{pg} for various species (Table 2). Using a range of d_{pg} consistent with observations, and a $\sigma_g = 2$, Figure 3 shows the L_m dependence on d_{pg} and R . In this case, particles in the accumulation and coarse modes tend to be scavenged quite efficiently even at a precipitation rate $R \sim 0.1 \text{ mm h}^{-1}$. Thus, for example, for $d_{pg} = 0.1 \mu\text{m}$, the aerosol lifetime varies between a fraction of an hour (for very intense rainfall) to several days (for weak rainfall). Ultimately, this analysis shows that L_m is strongly dependent on the precipitation rate R , which tends to determine the aerosol lifetime in precipitating clouds [Slinn, 1984; Giorgi and Chameides, 1986; Pruppacher and Klett, 1998].

3.3. Initial and Boundary Conditions

[18] The initial conditions for our model are provided by a meteorological sounding of temperature, horizontal wind components, and water-vapor mixing ratio, in the center of the domain of interest. In addition, aerosol vertical concentrations are given based on known surface measurements and assumed exponential decrease with altitude, with a characteristic height scale [d'Almeida et al., 1991]. The boundary conditions (BC) for the model include vertical profiles of the of potential temperature, water vapor mixing ratio, horizontal wind, and aerosol concentrations, as well as sea surface temperature (SST) for the lower boundary. Periodic lateral boundary conditions for all meteorological variables and a sponge-type condition

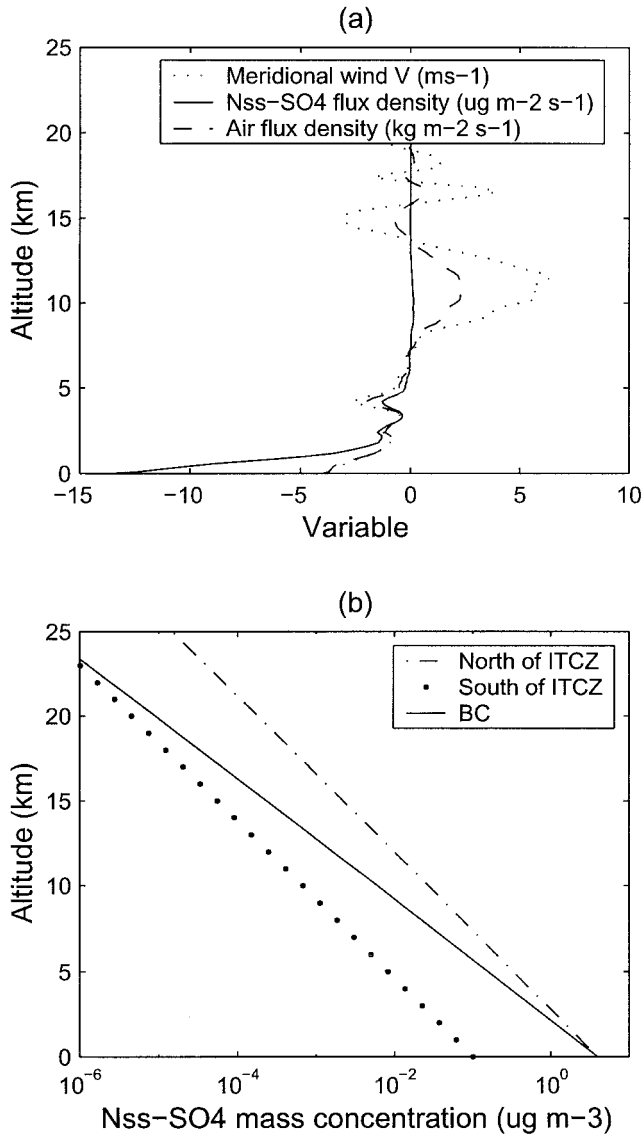


Figure 4. (a) Average vertical profile of mass flux density of nss-SO $_4$ aerosol (solid line), mass flux density of air (dashed line), and meridional wind V (dotted line), and (b) Vertical profiles of nss-SO $_4$ mass concentration north of the ITCZ (dash-dotted line), south of the ITCZ (dotted line), and the boundary condition profile used (solid line).

were applied at the top of the model domain to attenuate the gravity waves induced by convection.

[19] For the aerosol BC we provide a vertical profile that takes into account the origin of the air mass that enters the domain. Moreover, the BC is time-dependent to account for the average large-scale decay of aerosol in ITCZ as we illustrate in the next paragraph. To determine the BC aerosol profile for our domain, we note that, during the time interval simulated here, aerosols enter the domain in the lower troposphere in air masses from the Northern Hemisphere (NH). In the same time, cleaner air from the Southern Hemisphere (SH) enters the domain in the upper troposphere. A vertical profile of aerosol mass flux density into the domain is shown in Figure 4a for nss-SO $_4$. Almost all aerosol mass enters in the domain in the boundary layer (BL) ($z < 1$ km) with some contributions up to about 7 km. While the aerosol mass con-

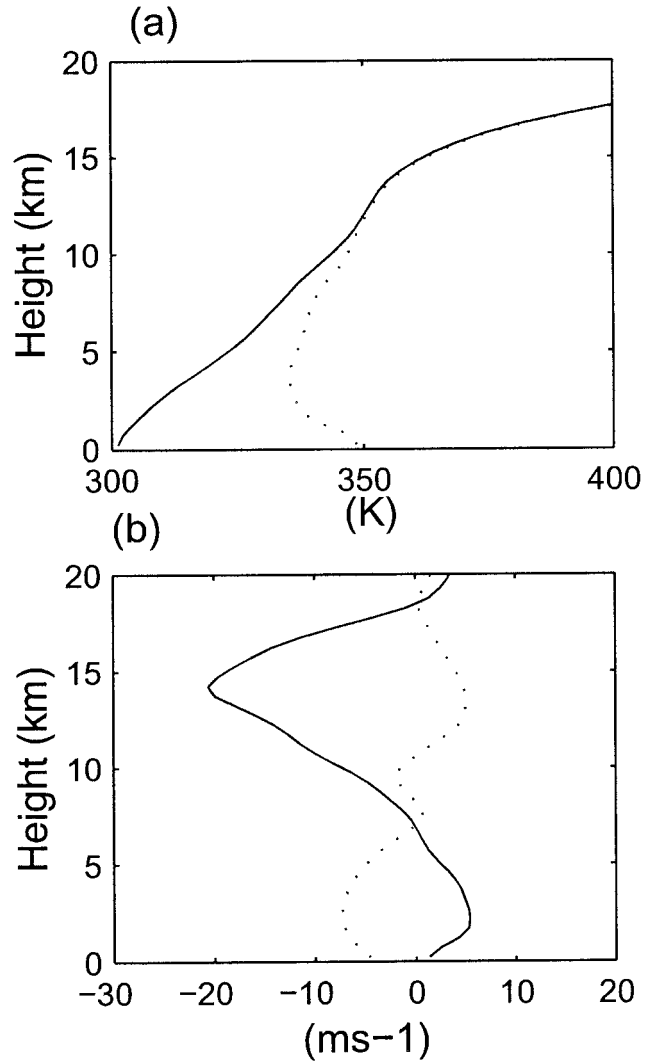


Figure 5. Initial vertical sounding from 16 March 1999, $t=0$ hour UT, from 5°S to 72°E, used to initialize the cloud-resolving model: (a) potential temperature (solid line) and equivalent potential temperature (dotted line), and (b) zonal wind component U (solid line) and meridional wind component V (dotted line).

tribution above 7 km is insignificant, the airflow from SH into the domain is important as shown by the air mass flux density above 7 km altitude. Thus, for the BC, we use a modified profile that resembles the aerosol profile north of ITCZ in the lower part of the atmosphere and resembles the aerosol profile south of ITCZ in the mid and upper (Figure 4b).

[20] On the basis of the data compiled in Table 1 and on reported aerosol measurements across the ITCZ during various phases of INDOEX, there is a large-scale aerosol mass concentration gradient across the ITCZ. In a first approximation the time average of this gradient is a result of the interactions between inflow of aerosol from the Northern Hemisphere (NH), precipitation removal, and mixing with other air masses. The mass concentration at surface can be approximated by $C(y) = C(0)\exp(-y/L_y)$, where y is the distance measured from the north of ITCZ toward south of ITCZ, L_y is a characteristic width of ITCZ (about 13° of latitude), so $L_y \sim 1.45 \times 10^6$ m, $C(0)$ is the surface aerosol mass concentration at

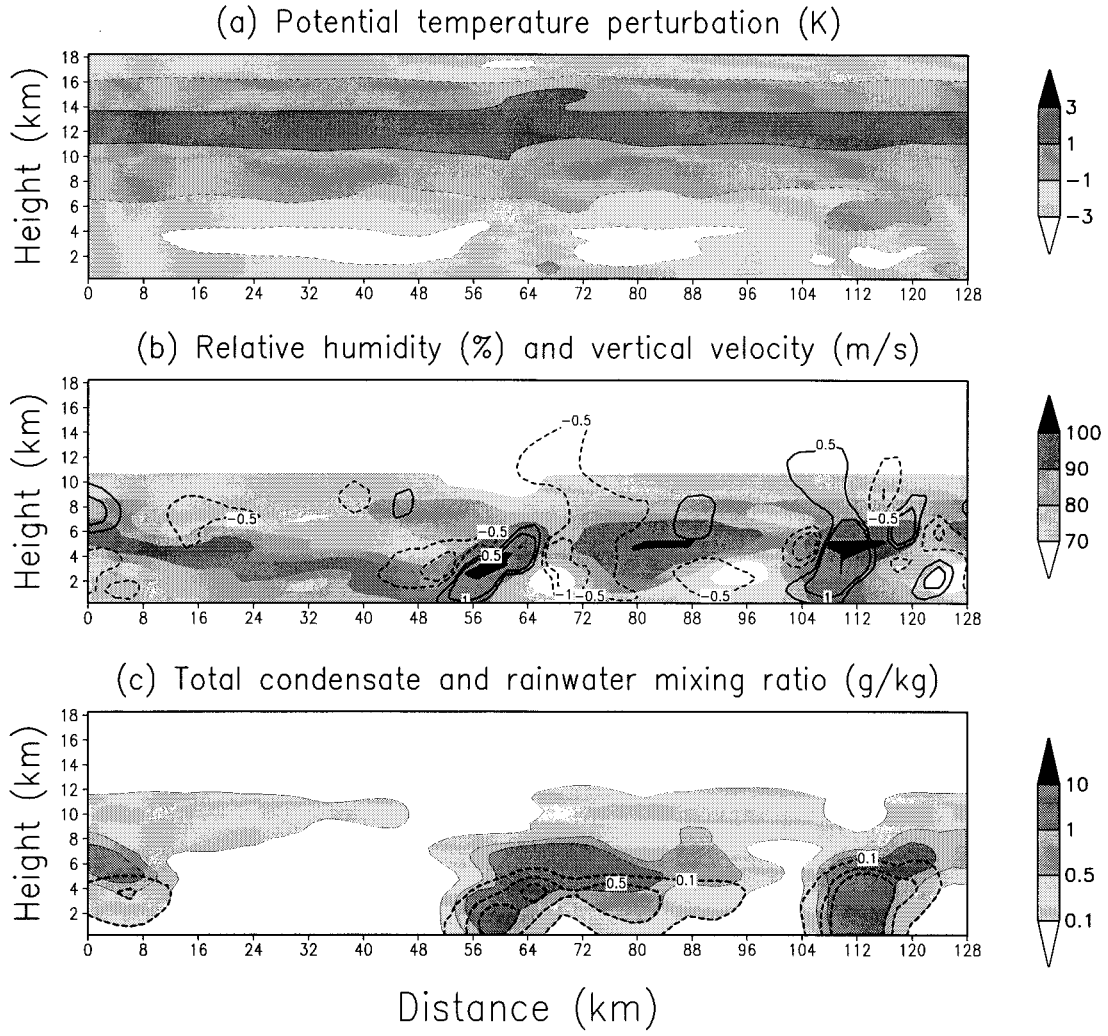


Figure 6. Instantaneous spatial distribution of model-simulated (a) potential temperature perturbation $\delta\theta$, (b) relative humidity (RH) (shaded areas) and vertical wind velocity W (solid lines for $W > 0 \text{ m s}^{-1}$ and dotted lines for $W < 0 \text{ m s}^{-1}$), and (c) total condensed cloud water and rainwater mixing ratio (dotted lines) at $t = 12 \text{ UT}$ of 16 March 1999, in a domain centered at 5°S – 72°E . (The plot corresponds to the model output after 12 simulated hours.)

north of ITCZ. For an average airspeed V toward south, $y = Vt$, and the large-scale variation of aerosol mass concentration can be represented as $C_{LS}(t) = C(0)\exp(-t/\tau_{LS})$, where for $-V = 2.8 \text{ m s}^{-1}$ we obtain a large-scale characteristic time $\tau_{LS} = 5.2 \times 10^5 \text{ s}$ for the case studied here. Observations show that mass concentration is dominant in the BL and decays with altitude with a characteristic height H (Figure 4b), $C(z, t) = C(0,0) \exp(-z/H) \exp(-t/\tau_{LS})$, which is given as BC.

[21] In addition, the effect of the large-scale flow on the dynamics of our domain has to be provided. The large-scale forcing terms are defined as functions of height and time and are based on the meteorological analysis provided by NCEP. The large-scale forcing treatment in this study follows the one described by Moncrieff *et al.* [1997] and includes the large-scale

advective tendencies of potential temperature, $\left(\frac{\partial \bar{\theta}}{\partial t}\right)_{LS}$, water mixing ratio, $\left(\frac{\partial \bar{q}}{\partial t}\right)_{LS}$, and the horizontal momentum, $\left(\frac{d\bar{V}}{dt}\right)_{LS}$. The large-scale average is indicated by overbar. The large-scale

advective tendencies for potential temperature θ and water mixing ratio q are

$$\left(\frac{\partial \bar{\theta}}{\partial t}\right)_{LS} \equiv -\bar{V} \cdot \nabla \bar{\theta} - W \frac{\partial \bar{\theta}}{\partial z} \quad (6)$$

$$\left(\frac{\partial \bar{q}}{\partial t}\right)_{LS} \equiv -\bar{V} \cdot \nabla \bar{q} - W \frac{\partial \bar{q}}{\partial z} \quad (7)$$

available at 6-hour intervals. These values are interpolated in height to the model's grid and in time to obtain values at each time step. The large-scale forcing term in the horizontal momentum equation is given by

$$\left(\frac{d\bar{V}}{dt}\right)_{LS} = \frac{\bar{V} - \bar{V}_{\text{obs}}}{t_a}, \quad (8)$$

where \bar{V} is the predicted large-scale horizontal velocity, \bar{V}_{obs} is the observed large-scale velocity, and t_a is an adjustment time

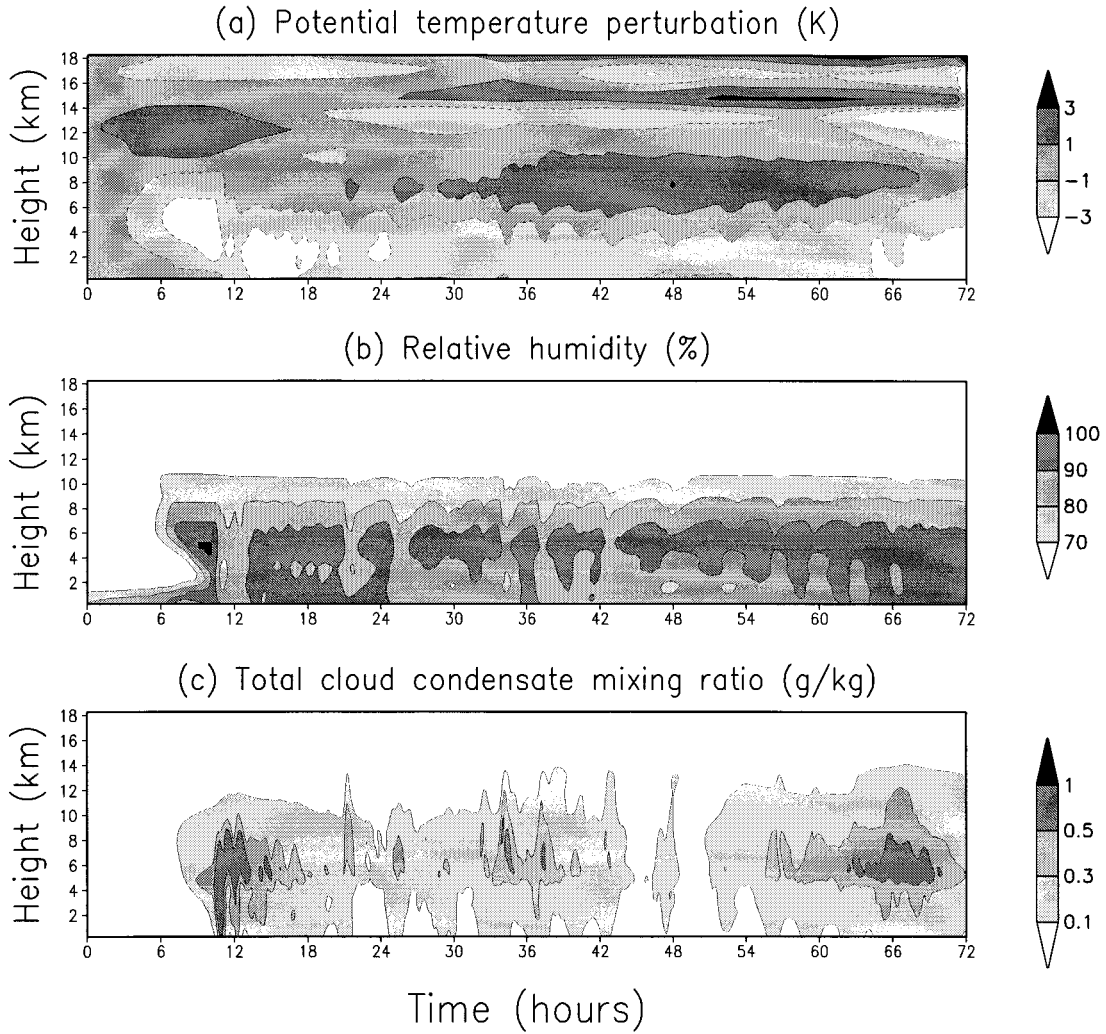


Figure 7. Time evolution of the horizontal average of (a) potential temperature perturbation $\delta\theta$, (b) relative humidity (RH), and (c) total cloud condensate mixing ratio $q_c + q_s + q_r$ for the time interval 16–18 March 1999.

($t_a = 7200$ s) [Moncrieff *et al.*, 1997]. By using this procedure the predicted horizontal wind does not depart too much from observations. The lower boundary of the model is an ocean surface, with the sea surface temperature (SST) from observations. The observed values at 6-hour intervals are interpolated and applied at each time step to determine the large-scale fluxes. The convection is initiated by applying small random perturbations in the potential temperature with a maximum magnitude of 0.5 K in the boundary layer (BL). This procedure was applied successfully by Moncrieff *et al.* [1997], Andronache *et al.*, [1999], and Donner *et al.*, [1999], producing realistic physical fields for convective systems in tropical area. Once the convective cells are formed, their evolution is controlled by the internal dynamics of the model and by the large-scale forcing.

4. Results and Discussion

4.1. Convective Activity in the Indian Ocean ITCZ

[22] The model was initialized with the vertical sounding from $t=0$ hour UT, 16 March 1999 (Figure 5). Figure 5a shows the potential temperature (solid line), and the equivalent potential temperature (dotted line). The plot indicates that air is

conditionally unstable in the lower part of the troposphere, suggesting favorable conditions for convection and cloud formation. Figure 5b shows the zonal wind component (solid line), predominant westerlies in the lower troposphere, and easterlies in the mid and upper troposphere. The meridional wind component (dotted line) indicates that in the lower troposphere the air flows from the northern Indian Ocean. Generally, the development of convection requires conditions with increased moisture and horizontal wind convergence in the lower part of the atmosphere. This causes a “mechanical” forcing of upward motions of air masses that become saturated and form clouds. Another mechanism is the release of latent heat in regions with supersaturation that can induce convective instability.

[23] An example of instantaneous potential temperature perturbation, defined as $\delta\theta = \theta - \bar{\theta}$, where $\bar{\theta}$ is the large-scale average, and θ is the local value, is shown in Figure 6a for $t = 12$ hours UT, 16 March 1999. Typical patterns of $\delta\theta$, favorable for deep convection, show negative values in the lower troposphere and positive values in the upper troposphere, similar with the $\delta\theta$ distribution found in other tropical convective systems [Donner *et al.*, 1999]. Concurrent with this potential

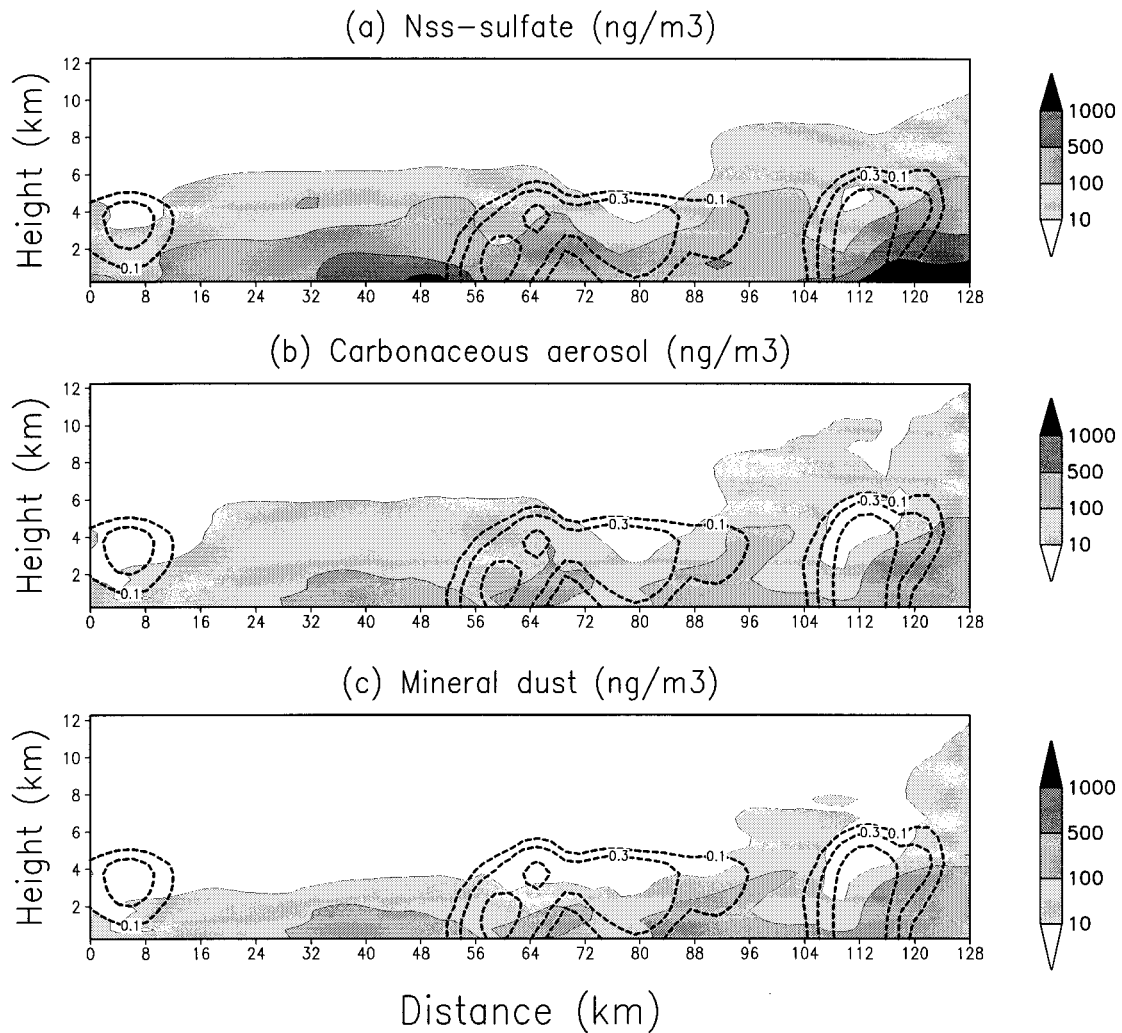


Figure 8. Example of instantaneous spatial distribution of model-simulated (a) nss-sulfate, (b) carbonaceous aerosol, and (c) mineral dust concentrations $t = 12$ UT of 16 March 1999. The rainwater mixing ratio q_r is shown in dotted lines.

temperature perturbation we observe the increase of relative humidity (RH) (Figure 6b) (shaded area). Overlapped in solid and dotted lines are shown the vertical velocity W intensity, and we note an increase of RH in updrafts ($W > 0 \text{ m s}^{-1}$) and a decrease of RH in downdrafts ($W < 0 \text{ m s}^{-1}$). These conditions produced two convective towers extending up to about 10 km, indicated by the distribution of total condensed water mixing ratio ($q_c + q_s + q_r$) (shaded areas) and by rainwater mixing ratio (q_r) (dotted lines) (Figure 6c). While this snapshot gives an idea about the spatial variability of variables in a convective domain, an overall view of the time evolution of variables of interest can be illustrated using horizontally domain averaged quantities. An example of time evolution of horizontally domain averaged quantities important for convection are shown in Figure 7. For all time interval simulated here, the lower troposphere tends to have perturbation of potential temperature, $\delta\theta < 0$, typically between -1° and -3°C (Figure 6a), which favors frequent increases of RH (Figure 7b). These conditions produced a total cloud condensate mixing ratio ($q_c + q_s + q_r$) shown in Figure 7c, with several rain events indicated by the isoline of 0.1 g kg^{-1} reaching the lower surface.

[24] The atmospheric circulation associated with the exam-

ple from 16 March, $t = 12$ hours UT, 1999, shows an instantaneous wind distribution with westerlies in the lower part of the troposphere, with intensities of a few meters per second and much stronger easterlies in the upper part of the troposphere (with intensities exceeding 20 m s^{-1}). The meridional wind shows consistent flow from the northern Indian Ocean in the lower troposphere (with intensities of $2\text{--}5 \text{ m s}^{-1}$) with a compensating flow toward the north in the upper troposphere. Under this airflow condition the polluted air masses are moving into the integration domain. These patterns of zonal and meridional flow are maintained during all time interval 16–18 March, 1999, consistent with the observations from aboard the *Ron Brown* ship (Figure 1) and with the NCEP data analysis. The vertical wind illustrated for this snapshot indicates intense updraft velocities in the cores of convective towers (W exceeding 3 m s^{-1}) and less intense downward velocities in the extended downdrafts between clouds. The circulation conditions in ITCZ created a total cloud cover of 75% and convective precipitation rates typically in the range $0.1\text{--}1.0 \text{ mm h}^{-1}$ with more intense rates in localized convective events. We must note that NCEP data exhibit somehow more intense precipitation rates and cloudiness between 5°S and 10°S , which sug-

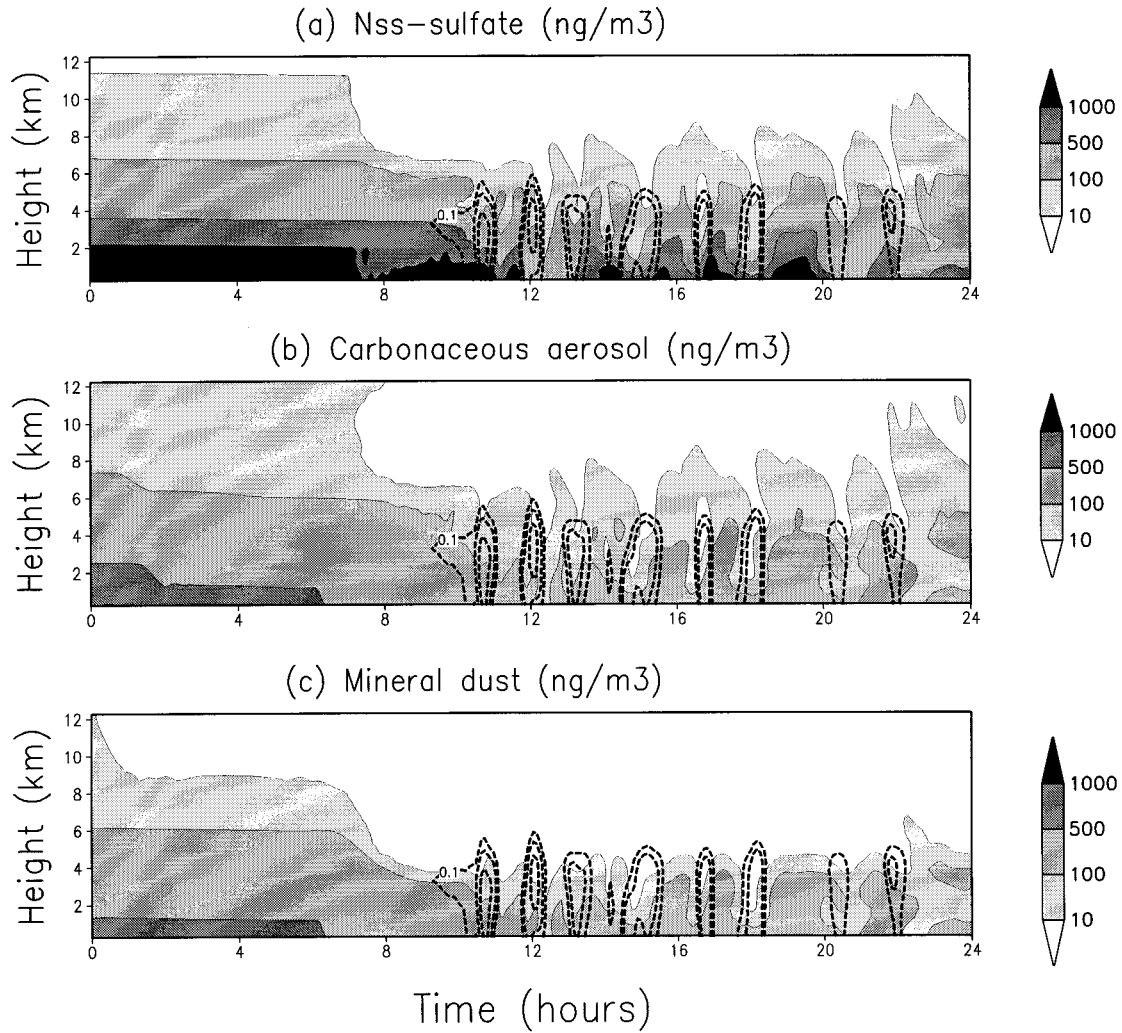


Figure 9. Time evolution of model-simulated (a) nss-sulfate, (b) carbonaceous aerosol, and (c) mineral dust concentrations for 16 March 1999, in the center of the domain. The rainwater mixing ratio q_r is shown in dotted lines.

gests that part of the aerosol traveling southward can be removed in these regions.

4.1.1. Aerosol Decay During Precipitation

[25] The spatial distribution of aerosol mass concentration for 16 March, $t=12$ hours UT, 1999, is shown in Figure 8. Generally, the nss-sulfate (shaded areas) concentration exhibits depletion in downdrafts as well as in areas with significant precipitation (indicated by the rainwater mixing ratio q_r , shown by dashed lines). Similar decay in aerosol mass concentrations are illustrated for carbonaceous particles (Figure 8b) and for mineral dust aerosol (Figure 8c), respectively. The time evolution of aerosol mass concentration in the center of the domain during 16 March 1999, is shown for nss-sulfate (Figure 9a), carbonaceous aerosol (Figure 9b), and mineral dust (Figure 9c). We note the gradual decrease of aerosol concentration and the negative correlation between aerosol concentration (shaded areas) and the rainwater mixing ratio q_r (dashed lines). For the entire time interval 16–18 March 1999, the total aerosol mixing ratio is contrasted with the rainwater mixing ratio q_r at surface for the point in the center of the domain (Figure 10a). This shows roughly the correspondence between the

sharp decay in aerosol concentration and the presence of a precipitation event. The aerosol lifetime is mainly determined by precipitation and mixing with air masses of various concentrations. We define an average aerosol lifetime τ by $dC/dt \sim -C/\tau$ at any atmospheric level, where C is the domain average concentration at that level. Thus the lifetime can be viewed as a characteristic time required to decrease the mass concentration e -fold from the initial concentration. This is a practical way to characterize aerosol residence at various levels and conditions. Correlation between C and precipitation rate in this study suggests that during time intervals with precipitation, τ is determined by precipitation removal, while when precipitation are lower or insignificant, the mixing is the factor determining the characteristic time. Figure 10b represents model-calculated aerosol mixing ratio at surface and mixing ratio decay corresponding to a lifetime of 1, 2, and 3 days. For all three simulated days the LAN simulated total aerosol mixing ratio is roughly between curves corresponding to lifetimes of 1 and 3 days, with significant variability especially during intense rain events. However, we must stress the variability in lifetime of aerosol due to intermittent character of convective precipitation, and the possibility that ITCZ can have time

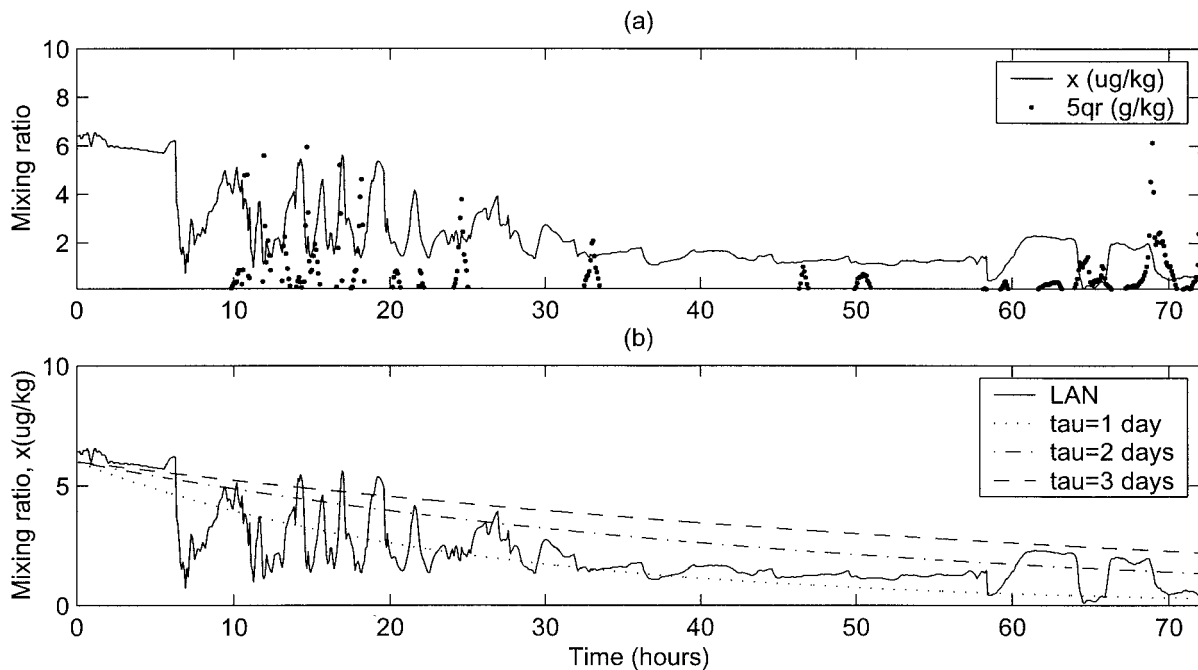


Figure 10. (a) Time evolution of model-simulated total aerosol mixing ratio (solid line) and rainwater mixing ratio q_r (solid circles) at surface, and (b) time evolution of model-simulated surface total aerosol mixing ratio (solid line) and aerosol mixing ratio exponential decay with characteristic times of 1, 2, and 3 days, for 16–19 March 1999, in the center of the domain.

intervals with weak precipitation or intense mixing as shown during the first simulated day.

[26] The time evolution of aerosol number concentration measured aboard of *Ron Brown* ship while crossing the ITCZ is shown in Figure 11a (solid line), and the latitude variation in time is given in Figure 11b. We note that the data are well represented by an exponential decay law with a lifetime between 2 and 3 days. The ship is moving southward (the latitude versus time is shown in Figure 11b) with a speed V_s , slightly faster than the average meridional wind at the surface, V . (Since the ship advances faster than the air mass, it will record a concentration gradient across the ITCZ that is larger than the real gradient that would be recorded during an ideal Lagrangian experiment.) Thus the observed concentrations on ship have to be adjusted to obtain what is called the “real” gradient in the polluted air mass. This adjustment is done considering the large-scale gradient of aerosol mass concentration at surface can be represented as $C(y) = C(0) \exp(-y/L_y)$ where L_y is a characteristic width of ITCZ, $y=Vt$, so that the real concentration across the ITCZ can be represented by $C_r(t) = C(0) \exp(-tV/L_y)$. The aerosol mass concentration observed by on the ship moving southward with a speed V_s is $C_s(t) = C(0) \exp(-tV_s/L_y)$. From these two relations we get $C_r(t) = C(0) \left(\frac{C_s(t)}{C(0)} \right)^b$ where $b = V/V_s$. For $V \sim 2.8 \text{ m s}^{-1}$ and $V_s \sim 5 \text{ m s}^{-1}$, $b = 0.56$, and we find that C_r is slightly smaller than C_s (shown as corrected data in Figure 11a). On the same plot are shown two curves corresponding to exponential concentration decay with characteristic times of 2 and 3 days.

[27] The time evolution of horizontally domain-averaged aerosol concentration during 16–18 March 1999, is shown in Figure 12. Figure 12a shows the time evolution of nss-sulfate concentration at $z = 0 \text{ km}$ (solid line), $z = 1 \text{ km}$ (dashed line), and $z = 3 \text{ km}$ (dash-dotted line). Similar evolutions are shown

for carbonaceous particles in Figure 12b and for mineral dust in Figure 12c. The results are in general agreement with the *Ron Brown* ship observations and with the inferred lifetimes

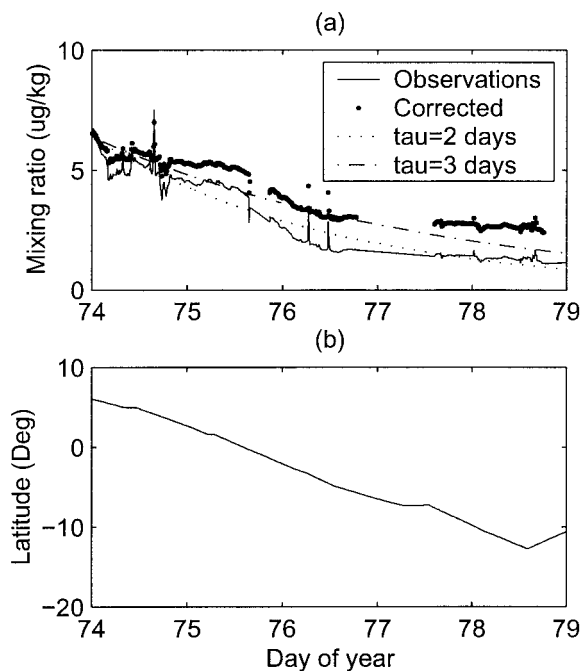


Figure 11. (a) Time evolution of total aerosol mixing ratio from ship observations. The original data are in solid line, and the corrected data are in solid circles. Exponential decay curves with characteristic times of 2 and 3 days are shown by dotted and dash-dotted lines, respectively. (b) Latitude versus time during the ship passage across the ITCZ.

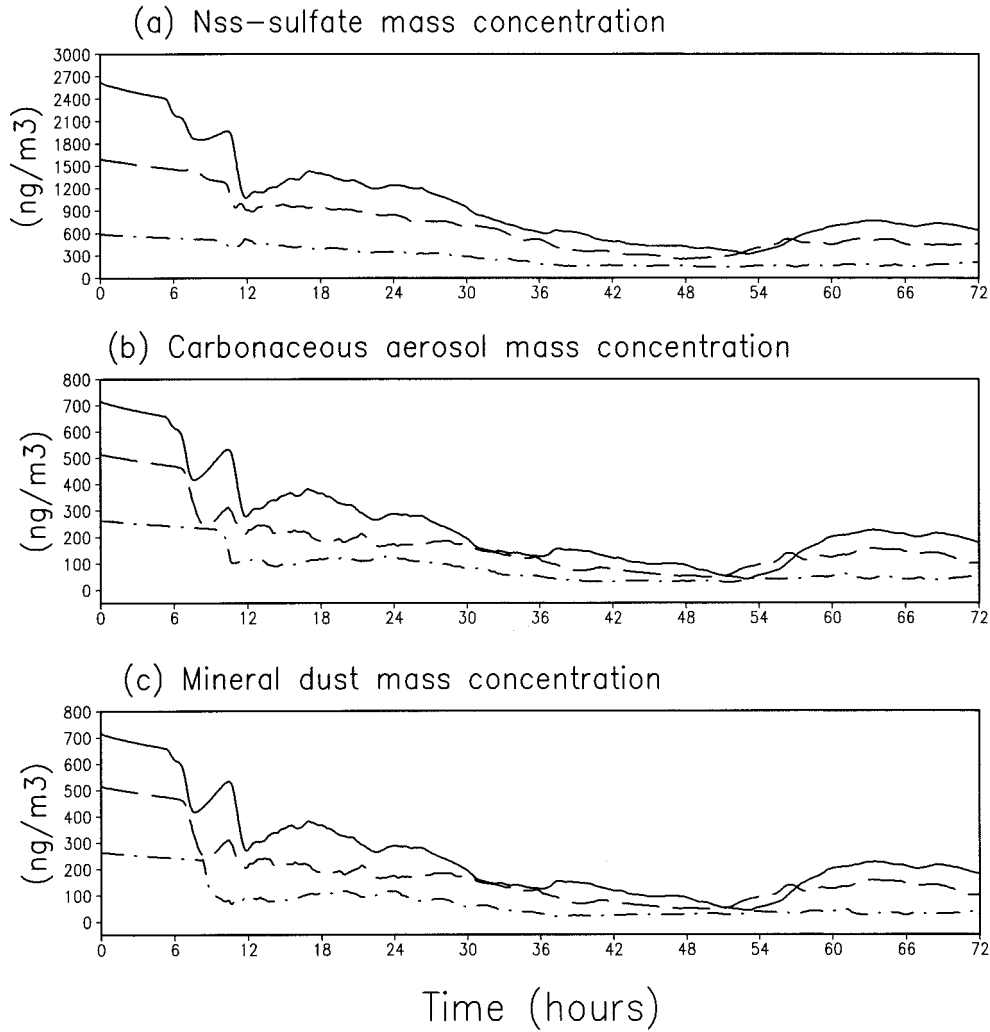


Figure 12. Time evolution of model-simulated (a) nss-sulfate, (b) carbonaceous aerosol, and (c) mineral dust concentrations for 16–19 March 1999. Here $z = 0$ km (solid line), $z = 1$ km (dashed line), and $z = 3$ km (dashed-dotted line). Quantities are horizontally domain-averaged.

(between 1 and 3 days) for the domain-averaged data or aerosol mass concentration at surface. These results are also consistent with the observed gradients in aerosol concentrations (Table 1). However, different scavenging efficiency of various aerosols can induce variability in lifetimes of carbonaceous particles for example. The assumption of aged aerosol insures that carbon-based aerosols are removed similar to sulfate-based particles. For fresher carbonaceous particles, model sensitivity shows that these particles tend to be longer-lived, and their removal becomes efficient only after they are sufficiently mixed with hydrophilic aerosols.

4.1.2. Aerosol Impact on Cloud Properties

[28] Previous studies indicated that an increase of aerosol concentration can cause an increase of cloud droplet number concentration and that for the same available atmospheric water content it could produce smaller droplets. The consequences of these processes are mainly an increase of cloud reflectivity of the shortwave radiation, but the complicated feedback between clouds and circulation can change the temperature, cloud lifetime, clouds, and precipitation distribution [Twomey, 1991; Penner *et al.*, 1994; Ackerman *et al.*, 2000;

Lohmann *et al.*, 2000]. An estimation of the impact of polluted air masses from north of ITCZ on the clouds in ITCZ was made by contrasting two runs that use the same meteorological initial conditions and large-scale forcing, but different aerosol loading. Run 1 uses aerosol loading corresponding to data from south of ITCZ, assumed to be representative for clean SH air masses. Run 2 used aerosol from the north of ITCZ, highly impacted by the pollution accumulated during winter monsoonal circulation (Table 1). We illustrate differences in effective radius of cloud droplets, r_e , number concentration of cloud droplets, N_d , and changes in cloud water mixing ratio q_c . Figure 13a shows that in contrast with Run 1 (clean conditions), the Run 2 (polluted conditions) shows a decrease of r_e by $\sim 2\text{--}3$ μm . The average decrease in r_e is -1.8 μm with a standard deviation of 1.5 μm . Similar changes were reported based on direct observations during INDOEX 1999. Thus Heymsfield and McFarquhar [2001] showed that the r_e decreased roughly by ~ 2 μm in a polluted cloud case versus a nonpolluted cloud case. Figure 13b shows that transition from clean to polluted scenarios causes an increase of the cloud droplet number density N_d by $40\text{--}100$ cm^{-3} , with an average of 67 cm^{-3} and a standard deviation of 18 cm^{-3} , results that are

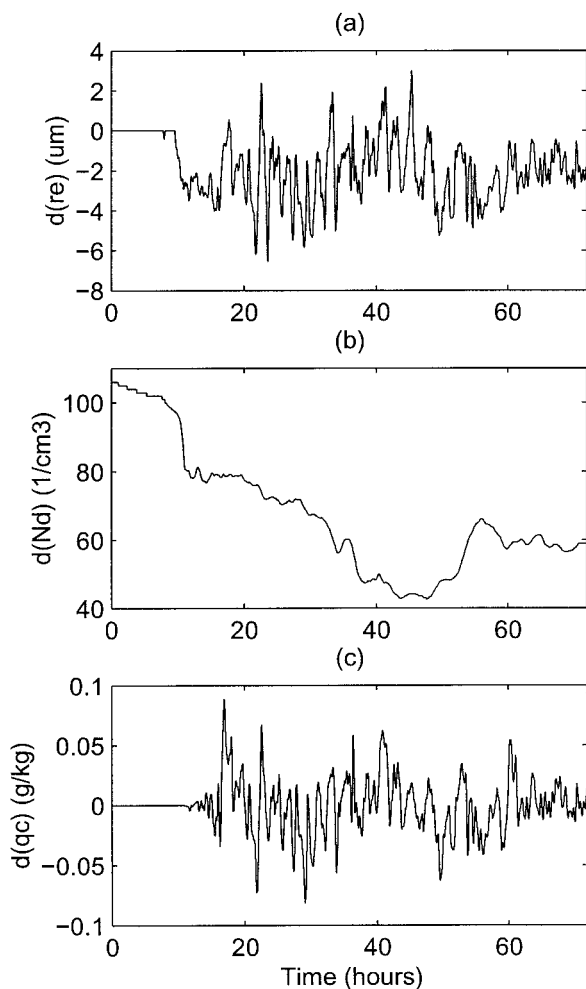


Figure 13. Time evolution of model-simulated changes between Run 1 (clean air mass) and Run 2 (polluted air mass) in (a) r_e , (b) N_d , and (c) q_c for 16–19 March 1999. Quantities are domain-averaged.

similar with observations by *Heymsfield and McFarquhar* [2001]. Simultaneous calculated variations of q_c are typically less than 0.02 g kg^{-1} (Figure 13c), with a negligible average of $-2 \times 10^{-4} \text{ g kg}^{-1}$ and a standard deviation of 0.02 g kg^{-1} . While the average of q_c over the integration domain for the three simulated days is negligible, the variability of this quantity is quite significant for short periods of time. The changes in r_e and N_d can be of relevance for cloud optical properties as shown in various previous studies treating the contrast between clean and polluted air masses [*Han et al.*, 1994; *Chuang et al.*, 1997].

[29] The optical depth of clouds, τ_c varies with the average effective radius as $\tau_c \sim 1/r_e$ for insignificant changes in liquid water path (LWP). Thus $\delta\tau_c/\tau_c = -\delta r_e/r_e$, and for $\delta r_e \sim -1$ to $-2 \mu\text{m}$, the relative increase in τ_c is ~ 10 – 20% , with a similar increase in cloud albedo. *Cantrell et al.* [2000] estimated the cloud condensation nuclei (CCN) concentration active at 0.5% supersaturation during a cruise through the Indian Ocean ITCZ. They found variations of ~ 1 order of magnitude in estimated CCN between north and south of ITCZ. It can be shown that $\tau_c \sim (N_d)^{1/3}$ where N_d is the cloud droplet number concentration, that tends to be proportional with CCN at the cloud base. This implies that for observed variations in CCN the changes in τ_c can be 10–30%, in qualitative agreement with

our estimations. These findings suggest that clouds in polluted air masses north of ITCZ are more reflective in shortwave (SW) radiation than clouds in pristine air masses south of ITCZ.

5. Conclusions

[30] During the winter monsoon conditions, large concentrations of aerosol of continental origin are transported over the northern Indian Ocean toward the tropical regions where they reach the ITCZ, a domain of fast processing of atmospheric particles. We used a high-resolution cloud-resolving model with aerosol-cloud interaction capabilities to explore the removal of sulfate, carbonaceous, and mineral dust aerosols in the Indian Ocean ITCZ deep convective systems. The main conclusions of this study are the following:

1. On the basis of NCEP meteorological data and aerosol concentrations measured north and south of the ITCZ, the model simulated 3 days of typical convective activity and precipitation regime, and the aerosol concentration decay due to precipitation removal and mixing was generally consistent with the observed surface aerosol concentration gradient across the ITCZ.

2. We found an average aerosol lifetime in the range 1–3 days in the boundary layer, consistent with calculations based on in situ measurements of aerosol concentration. Large variability in the aerosol lifetime can be induced by the variable precipitation regime, mixing processes, and by the nature of aerosol, such as hydrophilic properties of the aerosol surface and aerosol size distribution parameters.

3. Aerosol polluted air masses from the northern Indian Ocean can impact the cloud microphysical properties in the ITCZ convective systems. On the basis of this study, typical aerosol pollution during the winter monsoonal circulation can decrease the average cloud droplet effective radius r_e by about $2 \mu\text{m}$ and can increase the cloud droplet number density N_d by 40 – 100 cm^{-3} , in agreement with in situ observations.

[31] **Acknowledgments.** We are grateful to Andy Heymsfield, Greg McFarquhar, Bill Collins, Phil Rasch, and Tim Bates for discussions and help with the data. We thank Timothy Garrett and William Cooke for their thorough and thoughtful comments, which helped to improve the paper. Suggestions from two anonymous reviewers were very helpful and are highly appreciated.

References

- Ackerman, A. S., O. B. Toon, D. E. Stevens, A. J. Heymsfield, V. Ramanathan, and E. J. Welton, Reduction of tropical cloudiness by soot, *Science*, 288, 1042–1047, 2000.
- Andronache, C., L. J. Donner, V. Ramaswamy, C. J. Seman, and R. S. Hemler, Atmospheric sulfur and deep convective clouds in tropical Pacific: A model study, *J. Geophys. Res.*, 104, 4005–4024, 1999.
- Ansmann, A., D. Althausen, U. Wandinger, K. Franke, D. Müller, F. Wagner, and J. Heintzenberg, Vertical profiling of the Indian aerosol plume with six-wavelength lidar during INDOEX: A first case study, *Geophys Res. Lett.* 27, 963–966, 2000.
- Bates, T. S., D. J. Coffman, D. S. Covert, and P. K. Quinn, Regional marine boundary layer aerosol size distributions in the Indian, Atlantic, and Pacific Oceans: A comparison of INDOEX measurements with ACE-1, ACE-2, and AEROSOLS 99, *J. Geophys. Res.*, 107, 10.1029/2001JD001174, in press, 2002.
- Baumgardner, D., and A. Clarke, Changes in aerosol properties with relative humidity in the remote southern hemisphere marine boundary layer, *J. Geophys. Res.*, 103, 16,525–16,534, 1998.
- Cantrell, W., G. Shaw, C. Leck, L. Granat, and H. Cachier, Relationship between cloud condensation nuclei spectra and aerosol particles on a south-north transect of the Indian Ocean, *J. Geophys. Res.*, 105, 15,313–15,320, 2000.

- Chatfield, R. B., and P. J. Crutzen, Sulfur dioxide in remote oceanic air: Cloud transport of reactive precursors, *J. Geophys. Res.*, **89**, 7111–7132, 1984.
- Chuang, C. C., J. E. Penner, K. E. Taylor, A. S. Grossmann, and J. J. Walton, An assessment of the radiative effects of anthropogenic sulfate, *J. Geophys. Res.*, **102**, 3761–3778, 1997.
- Clarke, A., P. Quinn, and J. Ogren, INDOEX aerosol: A comparison and summary of microphysical, chemical, and optical properties observed from land, ship, and aircraft, *J. Geophys. Res.*, **107**, 10.1029/2001JD000572, in press, 2002.
- Collins, W. D., P. J. Rasch, B. E. Eaton, D. W. Fillmore, J. Kiehl, T. C. Beck, and C. S. Zender, Simulation of aerosol distributions and radiative forcing for INDOEX: Regional climate impact, *J. Geophys. Res.*, **107**, 10.1029/2000JD000032, in press, 2002.
- d'Almeida, G. A., P. Koepke, and E. P. Shettle, *Atmospheric Aerosols: Global Climatology and Radiative Characteristics*, 561 pp. A. Deepak, Hampton, Va., 1991.
- Dickerson, R. R., M. O. Andreae, T. L. Campos, O. L. Mayol-Bracero, C. Neusuess, and D. Streets, Emissions of black carbon and carbon monoxide from South Asia, *J. Geophys. Res.*, **107**, 10.1029/2001JD000501, in press, 2002.
- Donner, L. J., C. J. Seman, and R. S. Hemler, Three-dimensional cloud-system modeling of GATE convection, *J. Atmos. Sci.*, **56**, 1885–1912, 1999.
- Ebert, E. E., and J. A. Curry, A parameterization of ice cloud optical properties for climate models, *J. Geophys. Res.*, **97**, 3831–3836, 1992.
- Fitzgerald, J. W., W. A. Hoppel, and F. Gelbard, A one-dimensional sectional model to simulate multicomponent aerosol dynamics in the marine boundary layer, 1, Model description, *J. Geophys. Res.*, **103**, 16,085–16,102, 1998.
- Flossmann, A. I., and H. R. Pruppacher, The theoretical study of the wet removal of atmospheric pollutants, part II, The uptake and redistribution of $(\text{NH}_4)_2\text{SO}_4$ particles and SO_2 gas simultaneously scavenged by convective cloud using a two-dimensional cloud dynamics model, *J. Atmos. Sci.*, **45**, 1857–1871, 1988.
- Flossmann, A. I., H. R. Pruppacher, and J. H. Topalian, The theoretical study of the wet removal of atmospheric pollutants, part II, The uptake and redistribution of $(\text{NH}_4)_2\text{SO}_4$ particles and SO_2 gas simultaneously scavenged by growing cloud drops, *J. Atmos. Sci.*, **44**, 2912–2923, 1987.
- Garrett, T., P. V. Hobbs, and H. Gerber, Shortwave, single-scattering properties of Arctic ice clouds, *J. Geophys. Res.*, **106**, 15,155–15,172, 2001.
- Ghan, J. G., L. R. Leung, and R. C. Easter, Prediction of cloud droplet number in a general circulation model, *J. Geophys. Res.*, **102**, 21,777–21,794, 1997.
- Giorgi, F., and W. L. Chameides, Rainout lifetimes of highly soluble aerosols and gases as inferred from simulations with a general circulation model, *J. Geophys. Res.*, **91**, 14,367–14,376, 1986.
- Guazzotti, S. A., K. R. Coffee, and K. A. Prather, Continuous measurements of size-resolved particle chemistry during INDOEX-IFP 99, *J. Geophys. Res.*, **106**, 28,607–28,627, 2001.
- Han, Q., W. B. Rossow, and A. A. Lacis, Near-global survey of effective droplet radii in liquid water clouds using ISCCP data, *J. Clim.*, **7**, 465–497, 1994.
- Haywood, J. M., V. Ramaswamy, and L. J. Donner, A limited-area-model case study of the effects of sub-grid scale variations in relative humidity and cloud upon the direct radiative forcing of sulfate aerosol, *Geophys. Res. Lett.*, **24**, 143–146, 1997.
- Hegg, D. A., S. Rutledge, and P. V. Hobbs, A numerical model for sulfur chemistry in warm-frontal rainbands, *J. Geophys. Res.*, **89**, 7133–7147, 1984.
- Held, I. M., R. S. Hemler, and V. Ramaswamy, Radiative-convective equilibrium with explicit two-dimensional moist convection, *J. Atmos. Sci.*, **50**, 3909–3927, 1993.
- Heysfield, A. J., and G. M. McFarquhar, Microphysics of INDOEX clean and polluted trade cumulus clouds, *J. Geophys. Res.*, **106**, 28,653–28,674, 2001.
- Hobbs, P. V., and A. L. Rangno, Ice particle concentration in clouds, *J. Atmos. Sci.*, **42**, 2523–2549, 1985.
- Jayaraman, A., D. Lubin, S. Ramachandran, V. Ramanathan, E. Woodbridge, W. D. Collins, and K. S. Zalpuri, Direct observations of radiative forcing over the tropical Indian Ocean during the January–February, 1996 pre-INDOEX cruise, *J. Geophys. Res.*, **103**, 13,827–13,836, 1998.
- Krishnamurti, T. N., B. Jha, J. Prospero, A. Jayaraman, and V. Ramanathan, Aerosol and pollutant transport and their impact on radiative forcing over the tropical Indian Ocean during the January–February 1996 pre-INDOEX cruise, *Tellus, Ser. B*, **50**, 521–542, 1998.
- Lipps, F. B., and R. S. Hemler, Numerical simulation of deep tropical convection associated with large-scale convergence, *J. Atmos. Sci.*, **43**, 1796–1816, 1986.
- Lohmann, U., J. Feichter, J. Penner, and R. Leaitch, Indirect effect of sulfate and carbonaceous aerosols: A mechanistic treatment, *J. Geophys. Res.*, **105**, 12,193–12,206, 2000.
- Lord, S. J., H. E. Willoughby, and J. M. Petrowicz, Role of parameterized ice-phase microphysics in axisymmetric, non-hydrostatic tropical cyclone model, *J. Atmos. Sci.*, **41**, 2836–2848, 1984.
- Mari, C., D. J. Jacob, and P. Bechtold, Transport and scavenging of soluble gases in a deep convective cloud, *J. Geophys. Res.*, **105**, 22,255–22,267, 2000.
- Marshall, J. S., and W. M. Palmer, The distribution of raindrops with size, *J. Meteorol.*, **5**, 165–166, 1948.
- Moncrieff, M. W., S. K. Krueger, D. Gregory, J. Redelsperger, and W. Tao, GEWEX Cloud System Study (GCSS) working group 4: Precipitating convective systems, *Bull. Am. Meteorol. Soc.*, **78**, 831–845, 1997.
- Moody, J. L., et al., Precipitation composition and its variability in the southern Indian Ocean: Amsterdam Island, 1980–1987, *J. Geophys. Res.*, **96**, 20,769–20,786, 1991.
- Muller, D., F. Wagner, D. Althausen, U. Wandinger, and A. Ansmann, Physical properties of the Indian Ocean aerosol plume derived from six-wavelength lidar observations on March 25 1999 of the Indian Ocean Experiment, *Geophys. Res. Lett.*, **27**, 1403–1406, 2000.
- O'Dowd, C. D., J. A. Lowe, and M. H. Smith, Coupling sea-salt and sulphate interactions and its impact on the cloud droplet concentration predictions, *Geophys. Res. Lett.*, **26**, 1311–1314, 1999.
- Penner, J. E., et al., Quantifying and minimizing uncertainties of climate forcing by anthropogenic aerosols, *Bull. Am. Meteorol. Soc.*, **75**, 375–399, 1994.
- Podgorny, I. A., W. C. Connat, V. Ramanathan, and S. K. Satheesh, Aerosol modulation of atmospheric and surface solar heating over the tropical Indian Ocean, *Tellus, Ser. B*, **52**, 947–958, 2000.
- Prospero, J. M., Mineral and sea-salt aerosol concentrations in various ocean regions, *J. Geophys. Res.*, **84**, 725–731, 1979.
- Pruppacher, H. R., and J. D. Klett, *Microphysics of Clouds and Precipitation*, 714 pp., Norwell, Mass., 1998.
- Quinn, P. K., D. S. Covert, T. S. Bates, V. N. Kapustin, D. C. Ramsey-Bell, and L. M. McInnes, Dimethylsulfide/cloud condensation nuclei/climate system: Relevant size-resolved measurements of the chemical and physical properties of the chemical and physical properties of the atmospheric aerosol particles, *J. Geophys. Res.*, **98**, 10,411–10,427, 1993.
- Ramanathan, V., et al., Indian Ocean Experiment (INDOEX) white paper, C⁴, Scripps Inst. of Oceanogr., Univ. of Calif., San Diego, La Jolla, 1996.
- Ramaswamy, V., and J. T. Kiehl, Sensitivities of the radiative forcing due to large loading of smoke and dust aerosols, *J. Geophys. Res.*, **90**, 5597–5613, 1985.
- Rasch, P. J., et al., A comparison of scavenging and deposition processes in global models: Results from the WCRP Cambridge Workshop of 1995, *Tellus, Ser. B*, **52**, 1025–1056, 2000.
- Rhoads, K. P., P. Kelley, R. R. Dickerson, T. P. Carsey, M. Farmer, D. L. Savoie, and J. M. Prospero, Composition of the troposphere over the Indian Ocean during the monsoonal transition, *J. Geophys. Res.*, **102**, 18,981–18,995, 1997.
- Satheesh, S. K., V. Ramanathan, X. Li-Jones, J. M. Lobert, I. A. Podgorny, J. M. Prospero, B. N. Holben, and N. G. Loeb, A model for the natural and anthropogenic aerosols over the tropical Indian Ocean, *J. Geophys. Res.*, **104**, 27,421–27,440, 1999.
- Savoie, D. L., J. M. Prospero, and R. T. Ness, Nitrate, non-sea-salt sulfate, and mineral aerosol over the northwestern Indian Ocean, *J. Geophys. Res.*, **92**, 933–942, 1987.
- Scott, B. C., Predictions of in-cloud conversion rates of SO_2 to SO_4 based upon a simple chemical and kinematic storm model, *Atmos. Environ.*, **16**, 1735–1752, 1982.
- Seinfeld, J. H., and S. N. Pandis, *Atmospheric Chemistry and Physics*, 1326 pp., John Wiley New York, 1998.
- Slingo, A., A GCM parameterization for shortwave radiative properties of water clouds, *J. Atmos. Sci.*, **46**, 1419–1427, 1989.
- Slinn, W. G. N., Precipitation scavenging, in *Atmospheric Science and Power Production*, edited by D. Randerson, *DOE/TIC-27601*, pp. 466–532, U.S. Dep. of Energy, Springfield, Va., 1984.

- Slinn, W. G. N., L. Hasse, B. B. Hicks, A. W. Hogan, D. Lai, D. P. S. Liss, K. Munnich, G. A. Sehmel, and O. Vittori, Some aspects of the transfer of atmospheric trace constituents past the air-sea interface, *Atmos. Environ.*, *12*, 2055–2087, 1978.
- Taylor, G. R., S. Kreidenweis, and Y. Zhang, The effects of clouds on aerosol and chemical species production and distribution, 1, Cloud model formulation, mixing, and detrainment, *J. Geophys. Res.*, *102*, 23,851–23,865, 1997.
- Twomey, S. A., Aerosols, clouds and radiation, *Atmos. Environ., Part A*, *25*, 2435–2442, 1991.
- Wang, C., and P. J. Crutzen, Impact of simulated severe local storm on the redistribution of sulfur dioxide, *J. Geophys. Res.*, *100*, 11,357–11,367, 1995.
- Warneck, P., *Chemistry of the Natural Atmosphere*, 757 pp., Academic, San Diego, Calif., 1988.
- Warren, S. G., C. J. Hahn, J. London, R. M. Chervin, and R. L. Jenne, Global distribution of total cloud cover and cloud type amounts over ocean, *NCAR Tech. Note NCAR/TN-317+STR*, Natl. Cent. for Atmos. Res., Boulder, Colo., 1988.
- Weber, R. J., J. J. Marti, P. H. McMurry, F. L. Eisele, D. J. Tanner, and A. Jefferson, Measurements of new particle formation and ultrafine particle growth rate at a clean continental site, *J. Geophys. Res.*, *102*, 4375–4385, 1997.

C. Andronache, (corresponding author), Atmospheric and Environmental Research, Inc., 131 Hartwell Ave., Lexington, MA 02421-3126, USA. (andronac@bc.edu)

L. J. Donner, R. S. Hemler, and C. J. Seman, GFDL, NOAA, Princeton University, Princeton, NJ 08540, USA.